Chasing the Ideal Thermal Tracer in the Galactic Center

F. Mazoochi *[1], F.S. Tabatabaei[1,2], J. Ott[3], V. Ossenkopf-Okada[2], A. Brunthaler[4], S. Dzib[4], and Y. Gong[5]

[1]Institute for Research in Fundamental Sciences (IPM), School of Astronomy, Tehran, Iran
[2]I. Physik. Institut, University of Cologne, D-50937 Cologne, Germany
[3]National Radio Astronomy Observatory, P.O. Box O, 1003 Lopezville Road, Socorro, NM 87801, USA
[4]Max-Planck Institut für Radioastronomie, Auf dem Hügel 69, D-53121 Bonn, Germany
[5]Purple Mountain Observatory and Key Laboratory of Radio Astronomy, Chinese Academy of Sciences, Nanjing 210008, China

Abstract

The innermost kiloparsec of galaxies plays a critical role in driving their evolution. As the nucleus of our Galaxy, the Central Molecular Zone (CMZ) serves as a unique local laboratory for examining star formation and gas dynamics under extreme physical conditions. Due to severe optical dust extinction, radio and infrared observations are essential to disentangle its thermal and nonthermal components. In this study, we evaluate the H67α radio recombination line (RRL) observed with the Australia Telescope Compact Array (ATCA) as an extinction-free tracer of ionized gas across Sgr A, Sgr B, and the Radio Arc. Comparing H67α with 1.3 GHz MeerKAT radio continuum data reveals that assuming local thermodynamic equilibrium (LTE) and optically thin conditions overestimates the thermal free-free emission in parts of the RRL-detected regions. By analyzing the H67α/H66α line ratio and radio spectral indices, we show that this thermal excess is primarily driven by stimulated RRL emission in Sgr B1, whereas non-zero optical depth and optically thick conditions dominate in Sgr B2. Accounting for these physical conditions, we derive a median thermal fraction of 57.7% at 1.3 GHz in the dense ionized regions of the CMZ.

Keywords: *Galactic Center — ISM — Thermal and Nonthermal*

1. Introduction

Radio continuum (RC) emission provides key insights into the energy balance and structure formation of the interstellar medium (ISM) in galaxies (e.g., Tabatabaei et al., 2026). RC emission comprises thermal (free-free) radiation from warm ionized gas (H II regions, $S_\nu \propto \nu^{-0.1}$) and nonthermal synchrotron radiation from cosmic-ray electrons (CREs) spiraling in magnetic fields ($S_\nu \propto \nu^{\alpha_n}$) (Longair, 2010). Below ~10 GHz, the nonthermal component typically dominates in normal star-forming galaxies (Condon, 1992, Tabatabaei et al., 2017). Separating these two components is an essential first step toward understanding galactic evolution and cosmic-ray propagation.

Various techniques are used to separate thermal and nonthermal RC components. While multi-frequency assumptions and spectral energy distribution (SED) fitting with a constant spectral index are common (e.g., Klein et al., 1984, Meng et al., 2019), they often misestimate synchrotron emission due to cosmic-ray electron (CRE) energy losses (Longair, 2010). Similarly, infrared continuum proxies can overestimate free-free emission depending on local dust-heating mechanisms (e.g., Basu et al., 2012). Consequently, recombination lines, such as de-reddened Hα, provide the most reliable thermal tracers for resolved studies of ionized gas in galaxies (Tabatabaei et al., 2007).

Located in the Galactic Center (GC), the Central Molecular Zone (CMZ; $l = -1°$ to $1.5°$, $r \sim 250$ pc from Sgr A*) contains 3–5 $\times 10^7\, M_\odot$ molecular gas that is 5–10% of the total molecular gas in the entire galaxy (Dahmen et al., 1997). The CMZ exhibits highly diverse ISM environments and active star-forming complexes. In this study, we investigate the RC components and their physical conditions within Sgr A, Sgr B, and the Radio Arc regions. While Sgr A hosts the central supermassive black hole, Sgr B comprises Sgr B2, an intense starburst site with > 49 H II regions holding ~ 10% of the CMZ's gas (Gaume et al., 1995), and Sgr B1, an older region driven by evolved, dispersed ionized sources (Simpson et al., 2018). Adjacent

*famazoochi@ipm.ir, Corresponding author

doi: https://doi.org/10.52526/25792776-26.73.2-304

to Sgr A, the Radio Arc contains 40 pc-long nonthermal linear filaments alongside thermal arched filaments, the Sickle H II region, and the Pistol Nebula (Yusef-Zadeh et al., 1984).

Extreme optical extinction (A_V = 20–50 mag; Scoville et al. 2003) in the CMZ presents a major obstacle to studying thermal emission. Although Hα recombination line emission is a standard thermal tracer in optically thin regimes ($\tau_{\mathrm{H}\alpha} < 1$; Tabatabaei et al. 2007), it is entirely absorbed ($\tau_{\mathrm{H}\alpha} \gg 1$) towards the Galactic Center. Unattenuated by dust, radio recombination lines (RRLs) offer an ideal alternative for tracing free-free emission and measuring extinction in heavily obscured environments (Scoville et al., 2003). On the other hand, lower-frequency RRLs can be affected by maser amplification and non-LTE stimulated emission (Meng et al., 2019). High-frequency RRLs (e.g., H40α, H50α) and cm-wavelength lines (e.g., H90α, H100α) have been employed to trace thermal continuum, constrain electron temperatures and densities, and quantify extinction (Mazoochi et al., 2026, Scoville et al., 2003). In this work, we analyze the H67α line ($\sim$ 20 GHz) from the Survey of Water and Ammonia in the Galactic Center ((SWAG; Krieger et al., 2017)). Despite its potential as an extinction-free tracer, H67α remains relatively understudied, offering a fresh avenue to characterize the ionized gas across the CMZ.

2. Data

The MeerKAT L-band receiver provides one of the prominent radio RC maps of the CMZ. Encompassing approximately 6.5 deg^2 around the GC, this total intensity map is constructed from a hexagonal mosaic of 16 individual pointings. It delivers an angular resolution of 4″ at a central frequency of 1.3 GHz (Heywood et al., 2022), with an estimated calibration uncertainty of 5% (Knowles et al., 2022).

To determine the spectral index alongside the MeerKAT dataset, we incorporate 4.9 GHz RC observations from the Global View on Star Formation in the Milky Way (GLOSTAR) survey (Brunthaler et al., 2021, Gong et al., 2026, Medina et al., 2019). GLOSTAR is a C-band (4–8 GHz) radio continuum and spectral line survey covering Galactic longitudes from $-2°$ to $+60°$, conducted using the Karl G. Jansky Very Large Array (VLA) in conjunction with the Effelsberg 100-m telescope. The resulting map features a sensitivity of roughly 2 mJy beam^{-1} and an angular resolution of 18″.

Additionally, thermal emission is traced using the H67α RRL at 21.4 GHz, acquired from the SWAG using the Australia Telescope Compact Array (ATCA). This survey spans the entire CMZ across longitudes from approximately $-1°$ to $+2°$ within latitudes of $|b| \leq 0.4°$, maintaining a general flux density uncertainty of 15% (Krieger et al., 2017). Because certain regions of the H66α line at 22.4 GHz exhibit sidelobe artifacts, we limit its use to evaluating and comparing averaged RRL ratios instead of absolute intensities. The synthesized beam dimensions for the H67α and H66α data are 30.72″ × 20.60″ and 28.54″ × 19.39″, respectively, corresponding to a spatial resolution of about 1 pc.

All data are convolved to the lowest resolution (30″ × 20″ belongs to H67α RRL) and projected onto a common spatial grid using AIPS.

Flux uncertainties (σ) incorporate both calibration uncertainty (σ_{cal}) and map RMS noise (σ_{rms}), calculated as $\sigma = \sqrt{(F_\nu \times \sigma_{\mathrm{cal}})^2 + \sigma_{\mathrm{rms}}^2}$ and propagated through derived parameters. All uncertainties for reported mean values represent the standard error of the mean (the standard deviation divided by the square root of the sample size).

3. Separate Thermal and Nonthermal Emissions

In this section, we apply the TRT method utilizing RRLs to separate the thermal and nonthermal components of the MeerKAT 1.3 GHz CMZ map. Unlike shorter-wavelength recombination lines (e.g., Hα or Paα), RRLs are virtually unaffected by dust extinction, rendering them reliable tracers of free-free emission in the heavily obscured CMZ (Scoville et al., 2003). However, long-wavelength RRLs can be susceptible to non-LTE stimulation and masing effects, which can lead to an overestimation of the true thermal emission (Bendo et al., 2017, Gordon & Walmsley, 1990).

To test the reliability of RRL tracing at higher frequencies, we investigate the ATCA H67α RRL at 21.4 GHz. Assuming initial local thermodynamic equilibrium (LTE) conditions, we determine the emission measure (EM) from the integrated line intensity ($T_L \Delta v$, in K km s^{-1}) using the relation (Rohlfs & Wilson, 2013):

$$\frac{\mathrm{T_L}\Delta \mathrm{v}}{\mathrm{K,km,s^{-1}}} = 6.13\times10^{2}\left(\frac{\mathrm{T_e}}{\mathrm{K}}\right)^{-1.5}\left(\frac{\mathrm{EM}}{\mathrm{cm^{-6},pc}}\right)\left(\frac{\nu_\mathrm{L}}{\mathrm{GHz}}\right)^{-1}, \tag{1}$$

where $\nu_L = 21.4\,\mathrm{GHz}$ is the line frequency, Δv is the linewidth, and $\mathrm{T_e}$ is the electron temperature, for which we adopt a representative CMZ value of $T_e = 7500\,\mathrm{K}$. The continuum optical depth at $\nu_c = 1.3$,GHz (τ_c) is subsequently calculated from the EM via (Oster, 1961):

$$\tau_\mathrm{c} = 8.23\times10^{-2}\left(\frac{\mathrm{T_e}}{\mathrm{K}}\right)^{-1.35}\left(\frac{\mathrm{EM}}{\mathrm{cm^{-6},pc}}\right)\left(\frac{\nu_\mathrm{c}}{\mathrm{GHz}}\right)^{-2.1}. \tag{2}$$

The brightness temperature of the RC emission, T_c, is given by the radiative transfer equation, $\mathrm{T_c} = \mathrm{T_e}(1-\mathrm{e}^{-\tau_\mathrm{c}})$. In the Rayleigh-Jeans regime, $\mathrm{T_c}$ is then converted into thermal flux density. Subtracting this modeled thermal contribution from the observed 1.3 GHz continuum map yields the residual nonthermal flux density.

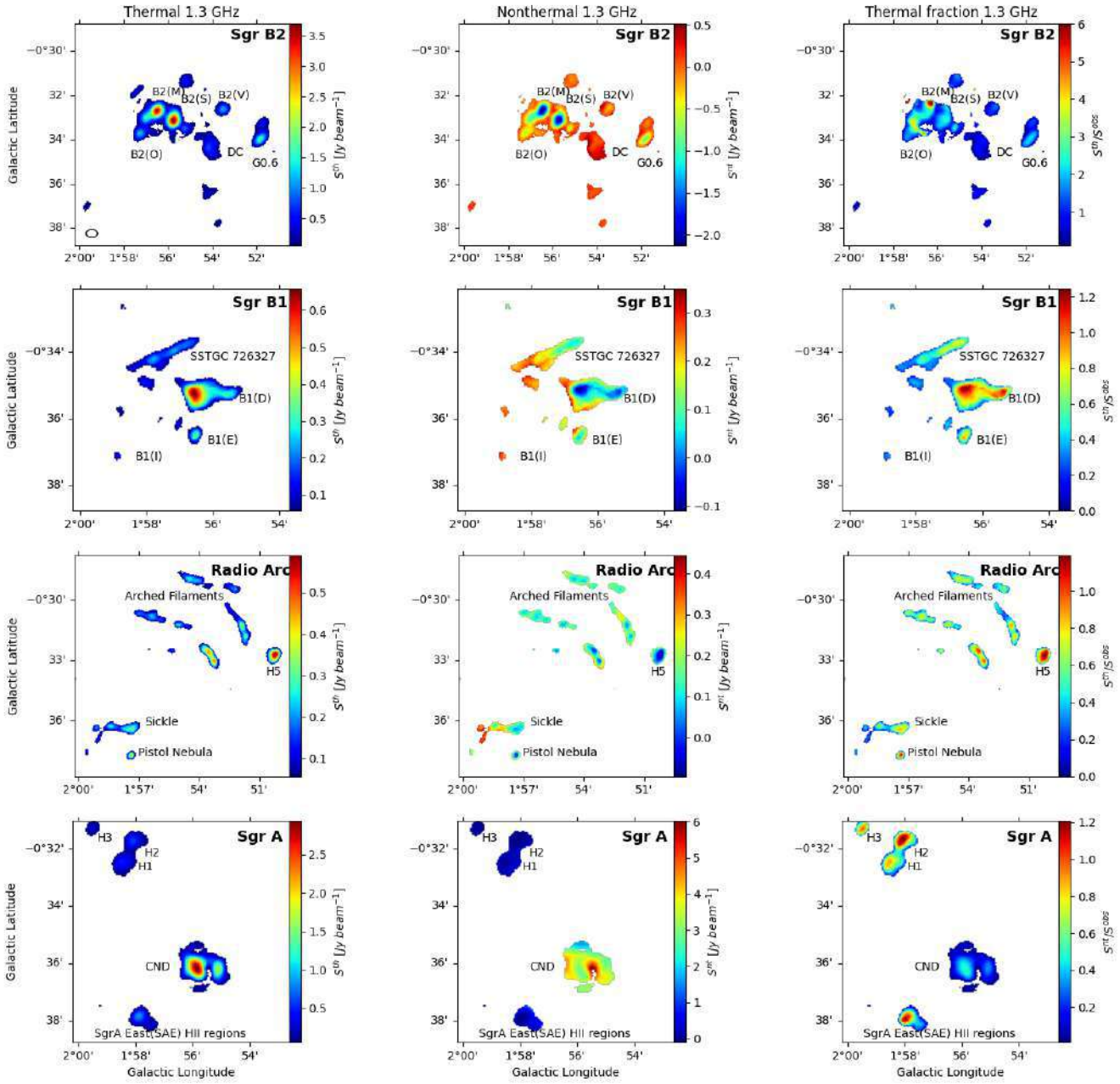

Figure 1. Maps of the 1.3 GHz thermal free-free emission (left), nonthermal synchrotron emission (middle), and thermal fraction (right) across the Sgr B2, Sgr B1, Radio Arc, and Sgr A regions. The synthesized beam size of $30'' \times 20''$ is indicated in the lower left corner of the Sgr B2 thermal map.

doi: https://doi.org/10.52526/25792776-26.73.2-304

Figure 1 displays the resulting thermal/nonthermal decomposition derived from the H67α RRL. In the brightest RRL-detected regions (highlighted in red on the thermal maps), the thermal continuum exceeds the total observed radio continuum, yielding unphysical negative nonthermal fluxes everywhere except at the center of Sgr A, where the radio continuum is exceptionally intense. This discrepancy indicates that the H67α line may also be subject to stimulation in select CMZ environments.

A primary source of uncertainty in this derivation is the adopted electron temperature. Across the Galactic Center, reported electron temperatures typically range between 5000 K and 10000 K (Gaume & Claussen, 1990, Lang et al., 2001), imparting an estimated $\sim$ 30% uncertainty on the median thermal emission fraction ($f^{\rm th}$). In Sgr A and the Radio Arc, where mean electron temperatures are reported as 6000 − 7000,K (Lang et al., 1997, 2001, Scoville et al., 2003), adopting $T_e < 7000$ K successfully eliminates the negative nonthermal residuals. Similarly, while Sgr B1 exhibits T_e variations between 6000 K and 9000 K (Mehringer et al., 1992, Simpson et al., 2018), adopting the lower bound of $T_e = 6000$ K yields $f^{\rm th} < 1$, resolving the negative nonthermal fluxes there as well. However, in the bright cores of Sgr B2, negative nonthermal components and high thermal fractions persist even at the lower limits of T_e uncertainty.

4. Radio Flux Ratios and the Spectral Index

To examine the physical conditions of these RRL-detected regions, we computed the relative spectral index ($\alpha = \log(S_1/S_2)/\log(\nu_1/\nu_2)$) using 1.3 GHz data from the MeerKAT telescope (Heywood et al., 2022) and 4.9 GHz data from the GLOSTAR survey (Brunthaler et al., 2021). Figure 2 presents the resulting α map across Sgr B2, Sgr B1, the Radio Arc, and Sgr A. Spectral index values between –0.1 and 2 generally denote thermal emission spanning optically thin to thick regimes, whereas values below –0.1 indicate optically thin non-thermal emission. The derived $\alpha_{1.3-4.9}$ distribution highlights distinct physical environments: Sgr B2 exhibits higher positive values ($\alpha > -0.1$), confirming optically thick thermal emission characteristic of an active star-forming region. In contrast, Sgr B1 and the Radio Arc average around $\alpha \approx -0.1$, consistent with optically thin thermal structures. While Sgr A shows predominantly steeper negative spectral indices overall, localized positive peaks trace the dense ionized emission surrounding Sgr,A* and nearby H,II regions.

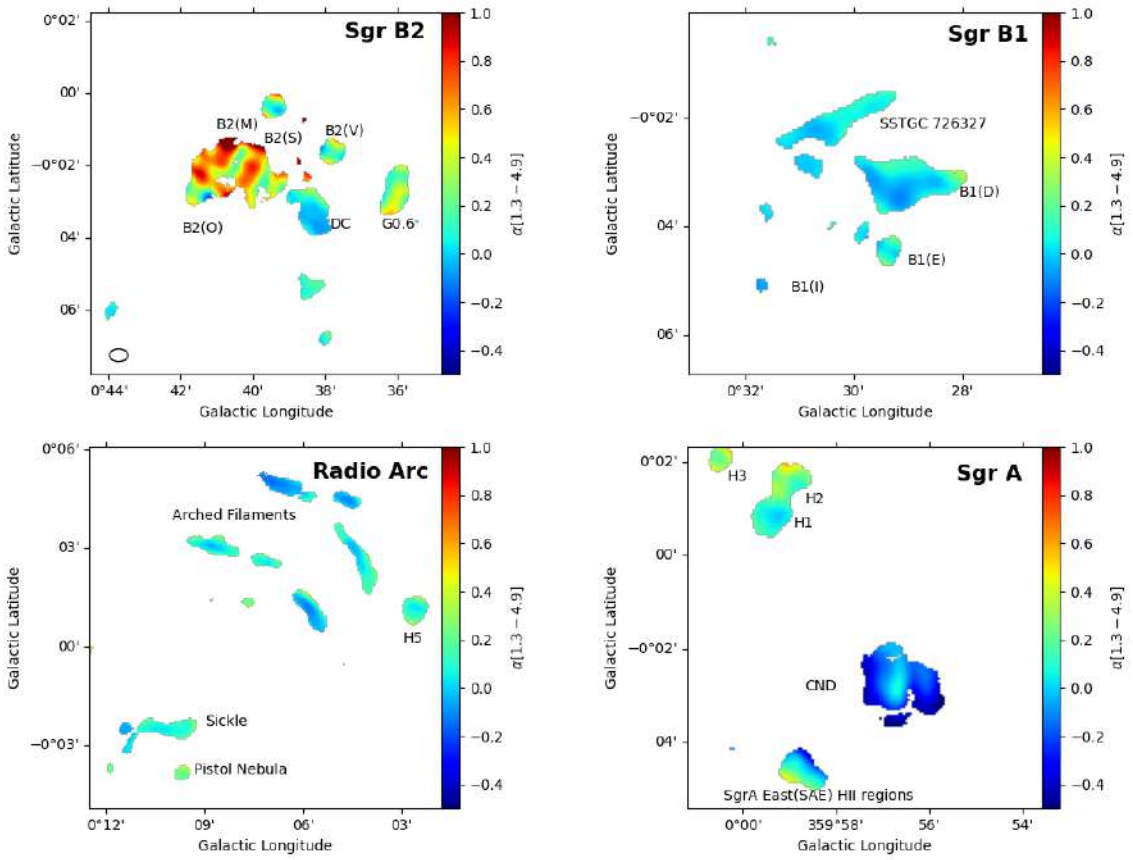

Figure 2. Spectral index ($\alpha_{1.3-4.9}$) map of the RRL-detected regions across Sgr B2, Sgr B1, the Radio Arc, and Sgr A, derived at a spatial resolution of $\sim$1 pc and clipped at the 3σ RMS noise level.

5. RRL ratio

To evaluate whether the H67α RRL serves as a reliable thermal tracer, we examine the normalized line ratio parameter $\eta = (\nu_{\rm H67}/\nu_{\rm H66}) \times (S_{\rm H66}/S_{\rm H67})$ using SWAG survey data. Values of $\eta < 1$ indicate this RRL stimulation, whereas $\eta = 1$ corresponds to local thermodynamic equilibrium (LTE) (Meng et al., 2019). Figure 3 presents η as a function of the thermal fraction ($f^{\rm th}$), color-coded by the 1.3 GHz MeerKAT spectral index (α_L), with binned median values (black dots) and 16th–84th percentile scatter bars. Overall, η decreases with increasing thermal fraction before flattening, exhibiting distinct regional behaviors.

In the dense star-forming cores of Sgr B2 ($f^{\rm th}_{1.3\,\rm GHz} > 1$), $\eta \approx 1$ and $\alpha_L > 0$, consistent with high electron densities driving level populations toward LTE in optically thick conditions (Gordon & Sorochenko, 2002, Mehringer et al., 1993); small-scale oscillations in η are attributable to residual H66α beam sidelobes. Across the extended, diffuse shells of Sgr B1, η drops below unity alongside $\alpha_L < 1$, signaling that RRL stimulation can lead to overestimates of the thermal fraction, though extremely low values may partly reflect instrumental recovery limits in diffuse gas. Within the Radio Arc, encompassing the Arched Filaments and Sickle HII region, the ratio remains near unity due to high electron densities ($n_e \sim 10^3$–$10^4\,{\rm cm}^{-3}$) maintained by ionizing radiation from nearby massive clusters (Lang et al., 2001), with only marginal non-LTE excursions ($\eta < 1$). Finally, Sgr A displays considerable scatter at low thermal fractions before converging toward $\eta \simeq 1$ and $\alpha_L \leq 0$. Here, localized enhancements in η arise from stimulated H66α emission driven by compact sources like Sgr A*, whereas instances of $f^{\rm th}_{1.3\,\rm GHz} > 1$ are sensitive to electron temperature assumptions (e.g., adopting $T_e = 6000\,{\rm K}$ reduces $f^{\rm th}_{1.3\,\rm GHz}$ below unity across Sgr A).

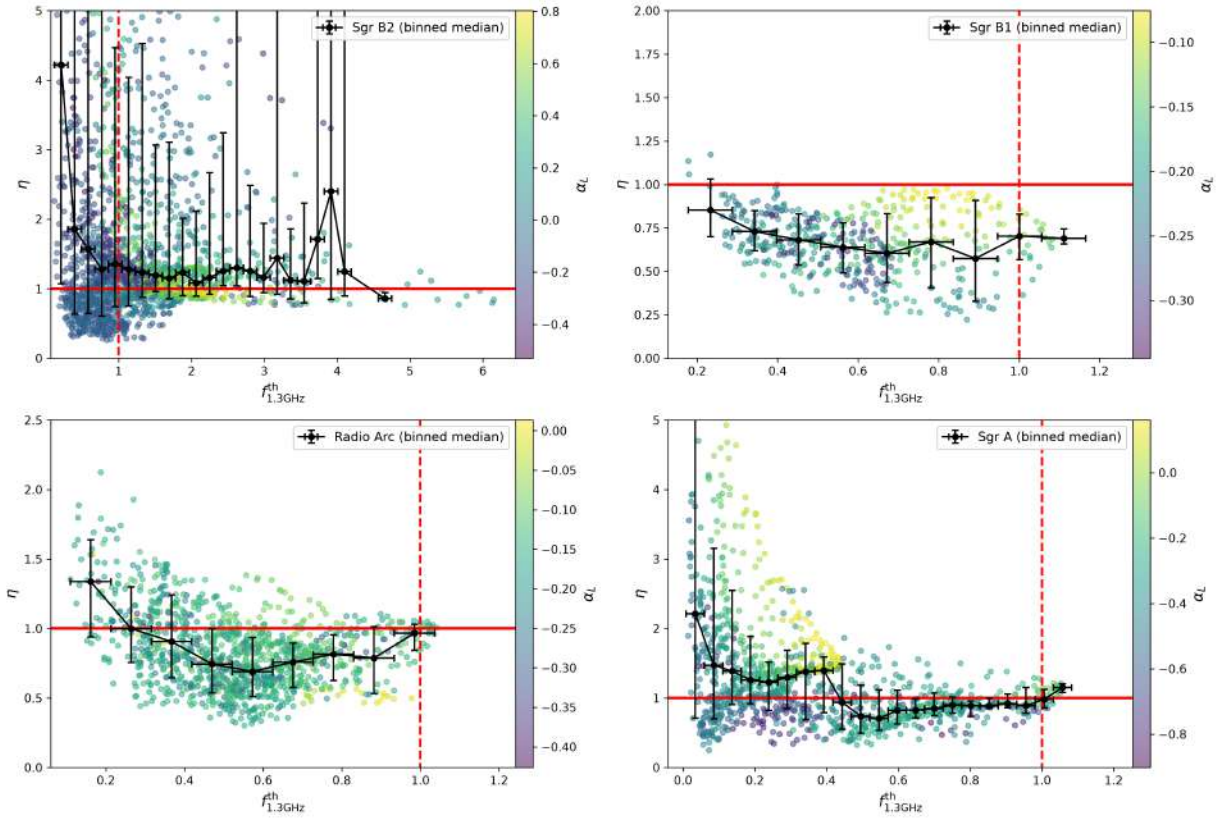

Figure 3. Scatter plots of η versus the $f^{\rm th}_{1.3\,\rm GHz}$ for Sgr B2, Sgr B1, the Radio Arc, and Sgr A, color-coded by the MeerKAT L-band spectral index ($\alpha_{\rm L}$). Connected black circles denote binned medians with 16th–84th percentile error bars. Red lines indicate $\eta = 1$ (solid horizontal) and $f^{\rm th}_{1.3\,\rm GHz} = 1$ (dashed vertical).

6. Summary and Conclusions

In this work, we investigate ionized regions traced by the H67α RRL to evaluate its efficacy as a thermal tracer within the complex environment of the GC. Using the TRT method applied to the MeerKAT 1.3 GHz RC map, we separated the thermal and nonthermal emission components. Our primary findings are summarized as follows:

- Deriving the 1.3 GHz nonthermal map via the H67α thermal emission reveals instances of negative nonthermal flux density. These anomalies are primarily driven by electron temperature uncertainties, RRL stimulation at 21.4 GHz, or local optical thickness in the 1.3 GHz RC map.
- The C- to L-band spectral index ($\alpha_{[1.3-4.9]}$) demonstrates that the star-forming Sgr B2 region, specifically the B2(M) and B2(S) pre-clusters, alongside select HII regions, are optically thick.
- Analysis of the H66α-to-H67α intensity ratio (η) indicates that the H67α RRL remains generally close to local thermodynamic equilibrium (LTE) in Sgr B2, Sgr A, and the Radio Arc. In contrast, the extended structures in Sgr B1 exhibit evidence of slight RRL stimulation ($\eta < 1$).

References

Basu A., Roy S., Mitra D., 2012, The Astrophysical Journal, 756, 141

Bendo G., Miura R., Espada D., Nakanishi K., Beswick R., D'Cruze M., Dickinson C., Fuller G., 2017, Monthly Notices of the Royal Astronomical Society, 472, 1239

Brunthaler A., et al., 2021, Astronomy & Astrophysics, 651, A85

Condon J., 1992, Annual review of astronomy and astrophysics, 30, 575

Dahmen G., Hüttemeister S., Wilson T., Mauersberger R., 1997, arXiv preprint astro-ph/9711117

Gaume R. A., Claussen M., 1990, Astrophysical Journal, Part 1 (ISSN 0004-637X), vol. 351, March 10, 1990, p. 538-562., 351, 538

Gaume R., Claussen M., De Pree C., Goss W., Mehringer D., 1995, Astrophysical Journal v. 449, p. 663, 449, 663

Gong Y., et al., 2026, Astron. Astrophys. , 706, A230

Gordon M. A., Sorochenko R. L., 2002, Radio recombination lines: their physics and astronomical applications. Astrophysics and Space Science Library Vol. 282, Springer Science & Business Media

Gordon M., Walmsley C., 1990, The Astrophysical Journal, 365, 606

Heywood I., et al., 2022, The Astrophysical Journal, 925, 165

Klein U., Wielebinski R., Beck R., 1984, Astron. Astrophys. , 135, 213

Knowles K., et al., 2022, Astronomy & Astrophysics, 657, A56

Krieger N., et al., 2017, The Astrophysical Journal, 850, 77

Lang C. C., Goss W., Wood O., 1997, The Astrophysical Journal, 474, 275

Lang C. C., Goss W. M., Morris M., 2001, The Astronomical Journal, 121, 2681

Longair M. S., 2010, High energy astrophysics. Cambridge university press

Mazoochi F., et al., 2026, The Astrophysical Journal, 997, 31

Medina S.-N. X., et al., 2019, Astron. Astrophys. , 627, A175

Mehringer D. M., Yusef-Zadeh F., Palmer P., Goss W., 1992, Astrophysical Journal, Part 1 (ISSN 0004-637X), vol. 401, no. 1, p. 168-181., 401, 168

Mehringer D. M., Palmer P., Goss W., Yusef-Zadeh F., 1993, Astrophysical Journal, Part 1 (ISSN 0004-637X), vol. 412, no. 2, p. 684-695., 412, 684

Meng F., et al., 2019, Astronomy & Astrophysics, 630, A73

Oster L., 1961, Reviews of Modern Physics, 33, 525

Rohlfs K., Wilson T. L., 2013, Tools of radio astronomy. Springer Science & Business Media

Scoville N., Stolovy S., Rieke M., Christopher M., Yusef-Zadeh F., 2003, The Astrophysical Journal, 594, 294

Simpson J. P., Colgan S. W., Cotera A. S., Kaufman M. J., Stolovy S. R., 2018, The Astrophysical Journal Letters, 867, L13

Tabatabaei F., Beck R., Krügel E., Krause M., Berkhuijsen E., Gordon K., Menten K., 2007, Astronomy & Astrophysics, 475, 133

Tabatabaei F., et al., 2017, The Astrophysical Journal, 836, 185

Tabatabaei F. S., et al., 2026, arXiv e-prints, p. arXiv:2606.27026

Yusef-Zadeh F., Morris M., Chance D., 1984, Nature, 310, 557